Line-on-Line Image Formation Analysis for Inkjet and Digital Fabrication Purposes

Trevor J. Snyder, Xerox Corp, Wilsonville, Yongkang Chen and Mark Weislogel, Portland State University, Portland, Oregon USA

Abstract

Many printing systems jet a material in liquid form which is subsequently cured or hardened prior to the next layer being applied. Examples include solid ink and UV curable ink systems and both have practical application in a variety of distinctly different business and industrial areas including printing, industrial fabrication processes and 3D printing. The fundamental building blocks of these devices are the formation and interaction of individual solidified dots and lines. Therefore, in the design and understanding of this technology, it is both essential and routine to evaluate and diagnose performance by studying the coalesced line formation within a jet and also the drop-to-drop and line-to-line formation from pass-to-pass. This paper presents both experimental and numerical results on the physics of liquid/solid inkjet droplet coalesces and dynamics.

Introduction

Many printing systems jet a material in liquid form which is subsequently cured or hardened. Examples include solid ink and UV curable ink systems and both have practical application in a variety of distinctly different business and industrial areas. For example, solid inks that change phase have been used for over two decades in Xerox's line of ColorQube solid ink products for the office and was recently introduced in the production space as the Xerox CiPress 325/500 Production Inkjet System. This robust head and ink technology is also currently used in a variety of digital fabrication applications including 3D printing and digital masking. Such technology has unique attributes which make it optimal for other applications as well.

The fundamental building blocks of this technology are the formation and interaction of individual solidified dots and lines. This is shown graphically in Fig. 1 for both primary and secondary lines.

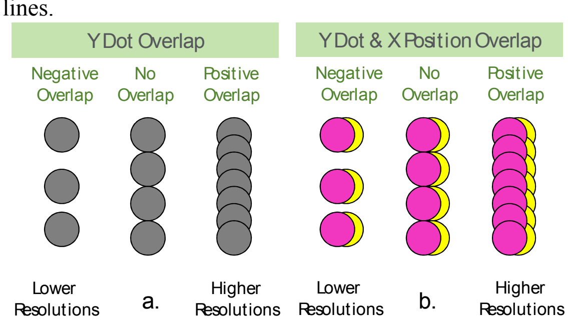

***Figure 1.** Fundamental dot and line patterns*

For solid ink systems, it has be shown [1] that solidification time scales are such that drops placed within an individual jet are completely molten, while drops placed from pass-to-pass are completely solidified. This is easily understood because the time between primary droplet depositions is given simply by (1/freq) (sec) which equates to drop-to-drop times ~0.05ms. The time from primary to secondary droplets is dependent on both the frequency and the spacing between jets, i.e., time = res·□x/freq. Fig. 2 shows these approximate times for a single and a multi-head architecture.

Color-To-Color	Multi-Head Architecture Spacing	Multi-Head Architecture Time Interval (ms)	Single Head Architecture Spacing	Single Head Architecture Time Interval (ms)
YK	Δx	14.9	Δx	0.415
CK	$2\Delta x$	29.7	$2\Delta x$	3.32
MK	$3\Delta x$	44.6	$3\Delta x$	3.37
CY	Δx	14.9	Δx	2.90
CM	Δx	14.9	Δx	0.415
MY	$2\Delta x$	29.7	$2\Delta x$	3.32

***Figure 2**. Time between droplet deposition*

Also, many systems operate in a scanning mode which leads to long line-to-line times and a UV cure is often performed between each imaging pass. These timescales and mechanical implementations result in liquid droplets impacting and interacting with the previously placed solid structures. Therefore, in the design and understanding of this technology, it is both essential and routine to evaluate and diagnose performance by studying the coalesced line formation within a jet and also the drop-to-drop and line-to-line formation from pass-to-pass.

Production inkjet, digital fabrication, and industrial marking applications are pushing inkjet systems into new frontiers of size, complexity and functionality, and these new systems are growing both in scale and in breadth of applications. There are systems now being designed and/or manufactured with tens of thousands and up to hundreds of thousands of jets. Also, these applications require a broad range of new materials to satisfy market requirements. New printheads have also been designed with higher frequency, smaller drops, and with new materials developed on a regular cadence. However, there are many other factors that impact the system performance and ultimately contribute to the desired customer needs in terms of quality, cost, and delivery. The topics are broad and include a need to build tools and understanding around the basic physics of material deposition and interaction. Sufficient understanding and design implementation of these system-level issues are as key to a successful product as is the primitive printhead performance metrics that are so heavily advertized.

©2013; Society for Imaging Science and Technology

Primary Line Topology Background

For the case of solid ink placed on a solid surface, it has been shown [2] that jetted molten drop line topographies can be predicted using

$$dpi_N = \frac{N}{2(\sin\theta + \pi(N-1)F_s/3F_c)}\left(\frac{\pi\rho F_s}{3m_d}\right)^{1/3} \tag{1}$$

where *dpi* is the dots per inch required to establish a variety of line topologies (N), m_d is the average mass of the drop, θ is the contact angle, and ρ is the ink density. The dimensionless term $F_s \equiv (1-\cos\theta)^2(2+\cos\theta)$ is a geometric wetting function characterizing in part the spherical end cap contributions, whereas $F_c \equiv 2\theta - \sin 2\theta$ is a geometric function characterizing in part the cylindrical drop body contributions. For this formulation, capillary dominance is assumed (small Bond number, $Bo = \rho g R^2/\sigma << 1$ where g and σ are gravity and surface tension, respectively) and the shape of the drop may be approximated by a spherical cap as shown in Fig. 3.

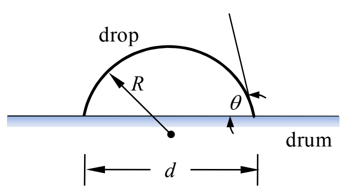

Figure 3. *Sketch of idealized Bo << 1 drop-on-drum.*

For $N = 1$ and $N = 2$, this equation predicts the isolated (i.e., single) and double-drop regimes, respectively.

$$dpi_{single} = \frac{1}{2}\left(\frac{\pi\rho F_s}{m_d \sin^3\theta}\right)^{1/3} \tag{2}$$

$$dpi_{double} = \frac{1}{(\sin\theta + \pi F_s/3F_c)}\left(\frac{\pi\rho F_s}{m_d}\right)^{1/3} \tag{3}$$

Taking $N \to \infty$, eq. (1) yields the minimum *dpi* for which a continuous line is formed; namely

$$dpi_{N\to\infty} \equiv dpi_{continuous} \gtrsim \frac{3F_c}{2\pi F_s}\left(\frac{\pi\rho F_s}{m_d}\right)^{1/3} \tag{4}$$

For *dpi* values above this incipient continuous line condition, the width of 'continuous lines' is expected to grow with increasing *dpi*. The line topologies are shown graphically in Fig. 4.

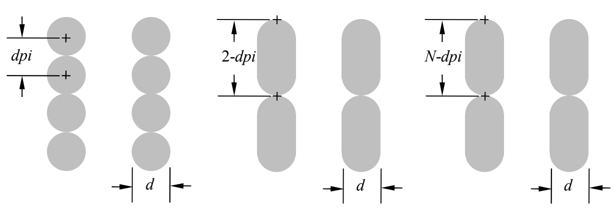

Figure 4. *Highest dpi setting for single drop (left), double-drop (middle), and N-drop (right) topological profiles.*

Therefore, Eq. (1) can be used to define various line topology regimes and limits as a simple function of drop mass, *dpi*, and temperature dependent properties ρ and θ. These results have been validated experimentally [2] and are shown visually in Fig. 5.

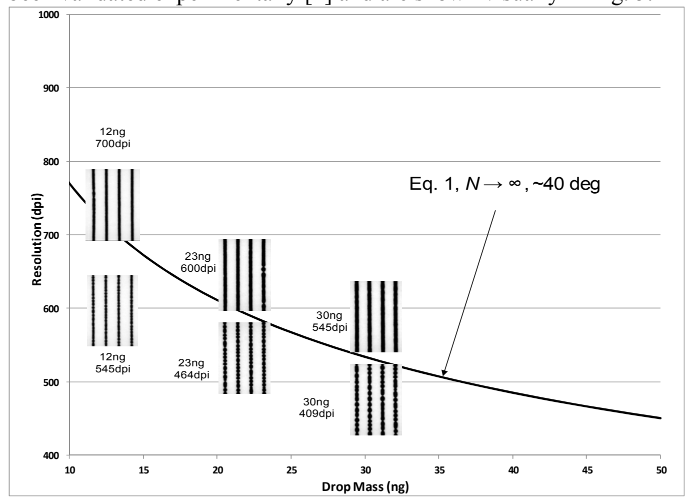

Figure 5. *Comparison of model for primary line formation*

Secondary Line Topology Results

In applications, drops and lines are not only formed on specific placement materials, but are placed on previously placed drops as in the case with secondary prin ted lines in inkjet printing as shown in Fig. 6.

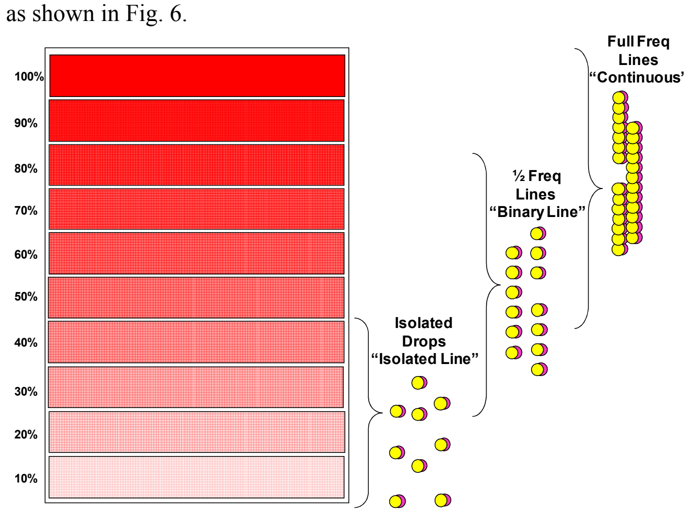

Figure 6. *Fundamental line composition of a printed image*

This is true for red, green, and blue secondary lines in graphics printers and is also true for the more fundamental mode of operation for a UV printer and even for a single component (monochrome) industrial application such as 3D printing. Compared to past work [2] this introduces many new variables including the important additional factor of x-axis position along with the various line structure physics that ultimately control the final solidified structure. From the empirical data in this study an interesting visual example can immediately be shown that compares the line structure between the primary line andsecondary line for different resolution and dropmass. This is shown in Fig. 7.

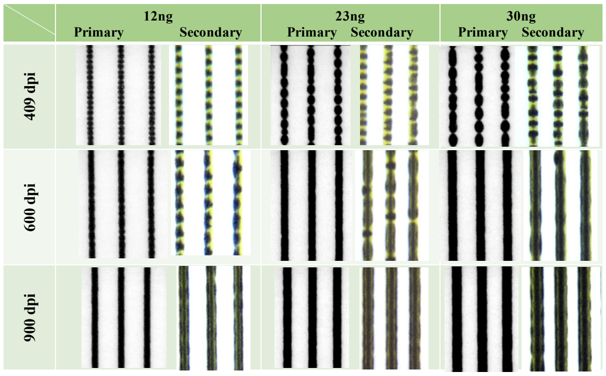

Figure 7. Primary and Secondary Line Structure

In this example, the data was created using black (dark) and yellow (light) ink for increased contrast. However, these results represent that which would be seen for any combination of primary and secondary lines. It can be seen from these pictures that the topology as predicted by Equation (1) is not the same between primary and secondary line structures given the same mass and resolution. Generally speaking the minimum *dpi* for which a continuous line is formed is increased, i.e., lines are still discontinuous in secondaries when the primary line would have achieved continuity. Results are shown in Fig. 8 that employs Eq. (1) effectively by simply introducing a larger contact angle.

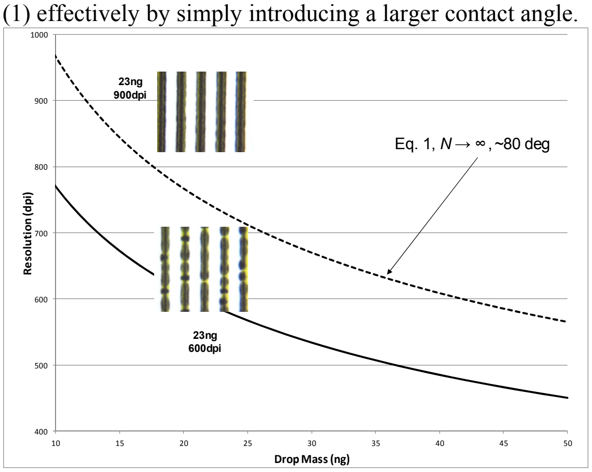

Figure 8. Comparison of model for secondary line formation

The model described by equation (1) and shown in Figure (5), does not satisfy Laplace's equation for a capillary surface of constant curvature and was created from observations that the projected surface area of two coalesced drops, hereafter referred to as a double-drop, has the same width as a single drop, *d*. Therefore, it was assumed that the projected 'double-drop' has a 'semi-pill-like' shape with boundaries consisting of two projected semi-circles of diameter *d* connected tangentially by a circular cylindrical body and with all contact lines satisfying the contact angle condition on the solid surface. Nonetheless, further support for its application is seen in Fig. 8 and its simplicity of application is intriguing and good enough for many practical purposes.

Secondary Line Topology Results

Related work [2] focused on primary line formation of which results are shown in Figures (3, 4 & 5). Besides the difference in individual line formation for the line-on-line or secondary structures as shown in Figures (6 & 7), one of the main new variables with secondary's is the combined impact of x- and y- dot and line position with the various line topologies. From this standpoint, line errors and even purposeful misalignments are known to be important in color inkjet printing for things such as banding and also digital fabrication applications. Any error can be magnified as a result of a liquid droplet interacting with a solid structure and this magnification has been termed dot position error amplification [3]. Adding to this work, this new study was performed in which the primary line quality was also varied by controlling the dpi and drop mass. This was done for controlled x-positional errors of 0, 25, 50, 75, and 100% overlap. The percent overlap is defined as the percentage offset (compared to 1/600dpi x-resolution) and is shown graphically in Fig 9. This study was performed over a wide range of drop masses (12, 24 & 30ng) and resolutions (400-1500dpi) similar to that done previously for primaries [2].

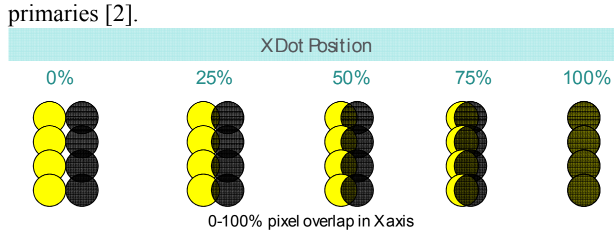

Figure 9. Primary and Secondary Line Structure

The primary variable of interest in this new work was the line-to-line structure created as a function of the different input variables. The results were three dimensional and many different measurement are possible. In this study a common banding measurement within Xerox was used called fsVBS or Full Spectrum Visual Band and Streak. It is a good tool to characterize both wide and narrow streaks. Higher numbers correspond to higher visual banding. Fig. 10 shows results for the fsVBS for the dropmass of 23ng (~23 pl) and over a wide range of resolution and percent overlap.

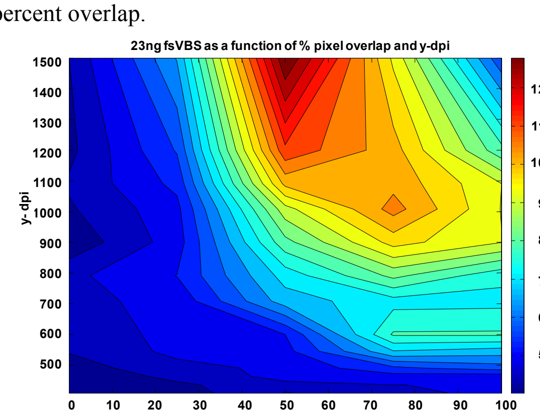

Figure 10. fsVBS Banding Measurement for 23ng lines

©2013; Society for Imaging Science and Technology

Similar trends were found for the other masses tested. There are a few interesting mechanisms at play as represented by the data in Fig.10. The low banding measurements on the left of the chart, i.e., areas of low overlap, represent a large misalignment of the lines. This misalignment leads to a very stable secondary line structure over the entire printed page and is a similar result as that shown by [3]. The low banding measurements on the bottom of the chart correspond to low dpi. In this region, there were observed dot structure variations, however, the variations were disperse and random and resulted in similar lightness and thus low banding. Dot error amplification was mitigated in this region. The high banding region (at high resolution and relatively large overlap) was caused from the instabilities of line-on-line formation. Some lines were perfectly overlapped and resulted in a dark band, while others were misaligned and resulted in a dramatically lighter band. This can be seen in Fig. 11.

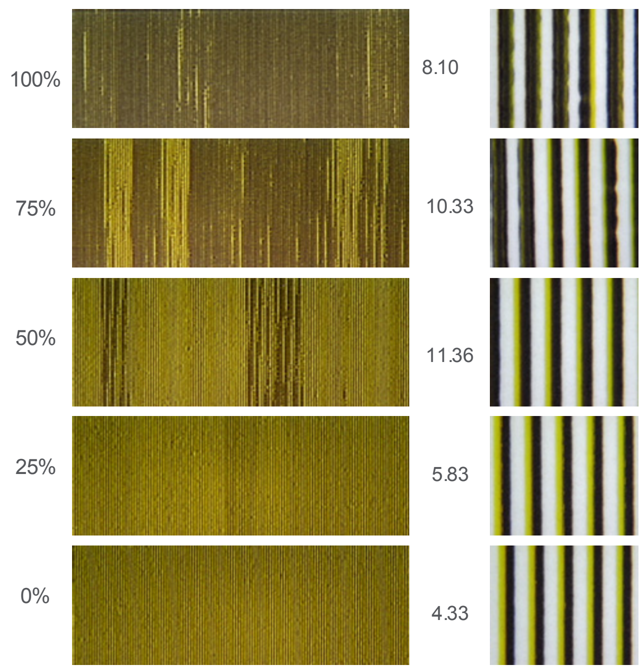

Figure 11. *fsVBS Banding Measurement for 23ng lines*

It is interesting that this dot error amplification was mitigated above about 1200dpi. For example, the upper right corner corresponds to the highest resolutions and largest overlap (exact line on line position). In this region the banding again decreased. This appeared to result from an advantageous spacing and placement which combined to form a uniform structure. This was not similarly measured for the 12ng drops in this region and occurred lower in resolution for the 30ng drops. Therefore, this appeared to be an interaction of position with coverage. One of the more important results from this data is the sensitivity of x position to banding which is an indicator of structural instability and/or consistency, i.e., we want low banding which corresponds to uniform structure. In this case, resolution was the most important variable, i.e. lower is better

In regions of low resolution, lines are formed from individual drops that interact with each other. In other testing, structural instabilities were measured in this region which did lead to significant structural non-uniformities and banding. The mechanism at play was that of "2D dot error amplification." This was aused equally from the instabilities caused from x or y errors and otherwise was similar to that previously shown by [3]. This is shown in Fig. 12 which plots a signal scoring transform (SST) for line quality as a function of the total x & y misalignment

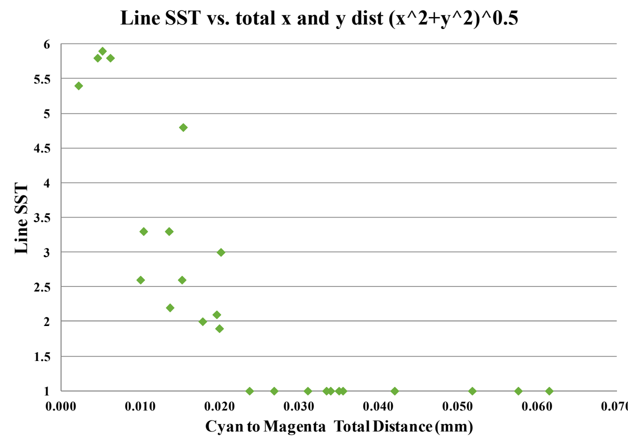

Figure 12. *Line SST measurement for low resolution line errors*

Fig. 13 is a visual example of the difference in density and line structure as represented in Fig. 12 between a line SST of 6 (left) and a line SST of 1 (right). Any error (x or y) resulted in a banded (light/dark) line as shown on the right. Very low error, as represented by the image on the left, resulted in droplets being placed directly on one another (darker density). Therefore, differences in position in either x or y across the page results in differences in structure and also banding. This behavior can only occur under certain circumstances and is unstable.

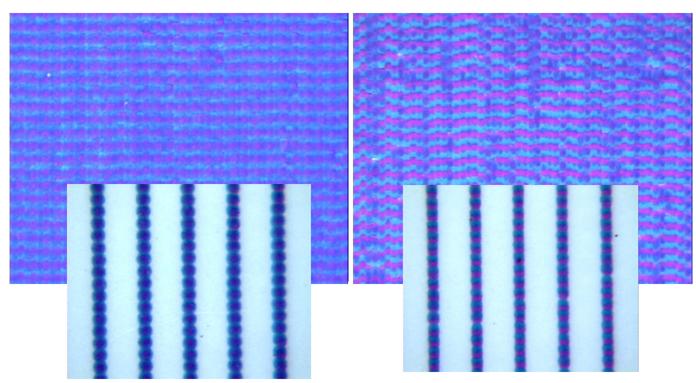

Figure 13. *Banding measurement for low resolution line errors*

Capillary Fluidics Modeling: SE-FIT Software

Capillary fluidics modeling of liquid on solid surfaces are shown which outline the different physics and outcomes for various length scales, droplet sizes, and surface and ink interface properties using the SE-FIT software open source design tool [4]. SE-FIT combines graphical user interfaces with the *Surface*

Evolver algorithm [5] to compute complex interfacial phenomena. It offers comprehensive functionalities for studying equilibrium capillary surfaces constrained by complex geometric boundaries. The results shown in Fig. 14 and 15 below are obtained with prebuilt models that enable a thorough exploration of the problem at hand.

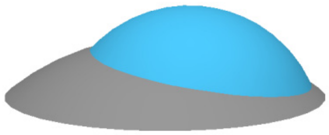

Figure 14. *Computed equilibrium configuration of a molten drop on a solidified drop with negligible gravity.*

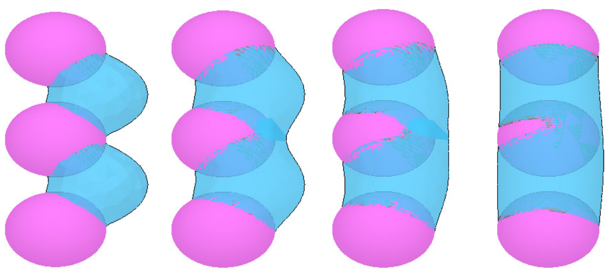

Figure 15. *From left to right, numerically computed interface configurations between two molten drops (cyan) and three solidified drops (magenta) leads to what appears as a characteristic 'banded line' segment. The equilibrium configuration is not unique as it depends on the spacing and the volume of the drops.*

Preliminary studies have been performed to examine elementary configurations resulting from the interactions between one molten drop and two solidified drops. Typical results are shown below as a function of spacing between the solidified drops and the volume ratio of the molten drop over that of the solidified drop.

s\vr	0.6	1	2
0.25	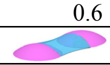	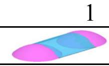	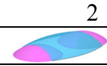
0.5			
1	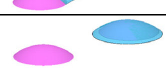	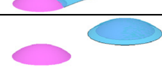	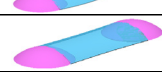

Figure 16. *Interface configurations as a function of spacing and volume ratio; s is the ratio of spacing over the drop base diameter d, vr is the volume ratio.*

The variation of curvature as a function of the spacing and the volume ratio is evident in Fig. 16. Furthermore, at large spacing and small volume ratio a stable configuration that connects the two solidified drops does not exist. The SE-FIT parameter sweep function enables us to identify a critical spacing for a given volume ratio and wetting condition. It is observed that the critical spacing is a weak function of wetting conditions and further research along this line is merited.

Conclusion

New industrial applications and competitive pressures are driving the demand for continued improvements to inkjet performance. Also, customer requirements are driving the need for new materials with dramatically different properties. To continue to improve the technology and achieve these demanding customer requirements, there is a need for better understanding of the fundamental imaging processes and the need for better measurement tools and methods. In this paper, mixed liquid-solid line structural results are shown both experimentally and numerically and a number of different results are presented. It is hoped that the results from this work reveal how an inkjet architecture is fundamentally different compared to other technologies and how different errors and material interactions may lead to various structural interactions with varying degrees of uniformity and functionality. This technology is quite different compared to other 3D printing technologies and also traditional aqueous inkjet technologies. Inkjet is a truly differentiated technology and is able to approach the market in unique ways to satisfy customer needs. Resolution, mass and positional errors can lead to different line qualities and have varying degrees of sensitivity to errors. If understood well, these errors can be used to ones advantage. If not, they can lead to numerous problems. Specifically, these results show the importance of deposition spacing and line placement error and order.

References

[1] T. Snyder, S. Korol, "Modeling the Offset Solid-Ink Printing Process," NIP 13, 1999.

[2] T. Snyder, N. Tavan, M. Weislogel, "Line Formation Analysis for Offset Solid Ink Printing", NIP 28, 2012.

[3] J. Padgett, R. Hill, "Methods to Mitigate Dot Position Error Amplification of Phase Change Inks", NIP 20, 2004

[4] Y. Chen, B.M. Schaeffer, M.M. Weislogel, G.A. Zimmerli, Introducing SEFIT: A Surface Evolver Based Tool for Studying Capillary Surfaces, AIAA-2011-1319, 11 pages, 49th AIAA Aerospace Sciences Meeting, 4-7 January 2011. The program is available at http://se-fit.com.

[5] K.A. Brakke, The *Surface Evolver*, *Experimental Mathematics*, Vol. 1, No. 2, 1992, pp. 141, 165, the code and manual are available at http://www.susqu.edu/facstaff/b/brakke/.

Author Biography

Dr. Trevor Snyder is a Mechanical Engineer and Principal Scientist working for Xerox in Wilsonville Oregon. Y. Chen and M.M. Weislogel are faculty at PSU with significant experience in large length scale capillary flow experiments. The three collaborate on science and engineering related to inkjet physics and devices.

This work was funded by a Xerox University Affairs Grant.